33RD INTERNATIONAL COSMIC RAY CONFERENCE, RIO DE JANEIRO 2013
THE ASTROPARTICLE PHYSICS CONFERENCE

ICRC 2013

New constraints on primordial black holes abundance from femtolensing of gamma-ray bursts

A. BARNACKA[1], J.-F. GLICENSTEIN[2], R. MODERSKI[1]

[1] *Nicolaus Copernicus Astronomical Center, Warszawa, Poland,*
[2] *DSM/IRFU/SPP, CEA/Saclay, F-91191 Gif-sur-Yvette, France*

abarnack@camk.edu.pl

Abstract: The abundance of primordial black holes is currently significantly constrained in a wide range of masses. The weakest limits are established for the small mass objects, where the small intensity of the associated physical phenomenon provides a challenge for current experiments. We used gamma-ray bursts with known redshifts detected by the Fermi Gamma-ray Burst Monitor to search for the femtolensing effects caused by compact objects. The lack of femtolensing detection in the data provides new evidence that primordial black holes in the mass range 10^{17} – 10^{20} g do not constitute a major fraction of dark matter.

Keywords: Femtolensing, PBHs, Compact Objects, GRBs.

1 Introduction

Dark matter is one of the most challenging open problems in cosmology or particle physics. A number of candidates for particle dark matter has been proposed over the years. An idea that the missing matter may consist of compact astrophysical objects was first proposed in the 1970s [1]. An example of such compact objects are primordial black holes (PBHs) created in the very early Universe from matter density perturbations. PBHs would form during the radiation-dominated era, and would be non-baryonic. That satisfy the big bang nucelosynthesis limits on baryons, and PBHs would be thus classified as cold dark matter in agreement with the current paradigm.

The abundance of PBH above 10^{15} g is a probe of gravitational collapse and large scale structure theory [2]. In particular, it constrains the gravitational wave background produced from primordial scalar perturbations in the radiation era of the early Universe [3]. Recent advances in experimental astrophysics, especially the launch of the FERMI satellite with its unprecedented sensitivity, has revived the interest in PBH physics [4].

Here, we present the results of a femtolensing search performed on the spectra of GRBs with known redshifts detected by the Gamma-ray Burst Monitor (GBM) on board the FERMI satellite [5]. The non observation of femtolensing on these bursts provides new constraints on the PBHs fraction in the mass range $10^{17} - 10^{20}$ g. We describe the optical depth derivation based on simulations applied to each burst individually. The sensitivity of the GBM to the femtolensing detection is also calculated.

2 Femtolensing

One of the most promising ways to search for PBHs is to look for lensing effects caused by these compact objects. Since the Schwarzschild radius of a PBH is comparable to the photon wavelength, the wave nature of electromagnetic radiation has to be taken into account. In such a case, the lensing caused by PBHs introduces an interferometry pattern in the energy spectrum of the lensed object [6]. Figure 1 shows a schematic picture of a femtolensing phenomena. This effect is called 'femtolensing' [7] due to the $\sim 10^{-15}$ arcseconds angular distance between the images of a source lensed by a 10^{18} g lens. The phenomenon has been a matter of extensive studies in the past [8], but the research was almost entirely theoretical since no case of femtolensing has been detected as yet. Gould (1992) [7] first suggested that the femtolensing of GRBs at cosmological distances could be used to search for dark matter objects in the $10^{17} - 10^{20}$ g mass range. Femtolensing could also be a signature of another dark matter candidate: clustered axions [9].

2.1 Magnification and spectral pattern

Consider the lensing of a GRB event by a compact object. In the case of a point source, the amplitude contributed by the $r_\pm$ images is

$$A_\pm \propto \frac{\exp(i\phi_\pm)}{\sqrt{|1-\frac{r_E^4}{r_\pm^4}|}}. \qquad (1)$$

The magnification A^2 is obtained by summing the amplitudes (1) and squaring, which gives

$$A^2 = |A_+ + A_-|^2 = \frac{1}{1-\frac{r_E^4}{r_+^4}} + \frac{1}{1-\frac{r_E^4}{r_-^4}} + \frac{2\cos(\Delta\phi)}{\sqrt{|1-\frac{r_E^4}{r_+^4}|}\sqrt{|1-\frac{r_E^4}{r_-^4}|}}, \qquad (2)$$

where r_E is the Einstein radius, r_+ and r_- are the distances between the lens and first and second image, respectively. Equation (2) indicates that the magnification depends on the phase. When the two lights paths are not temporally coherent equation (2) is reduced to the two first components.

In the case of femtolensing, the phase shift between the two images is:

$$\Delta\phi = \frac{E\,\delta t}{\hbar}, \qquad (3)$$

where E is the energy of the photon. The energy dependent magnification produces fringes in the energy spectrum of the lensed object.

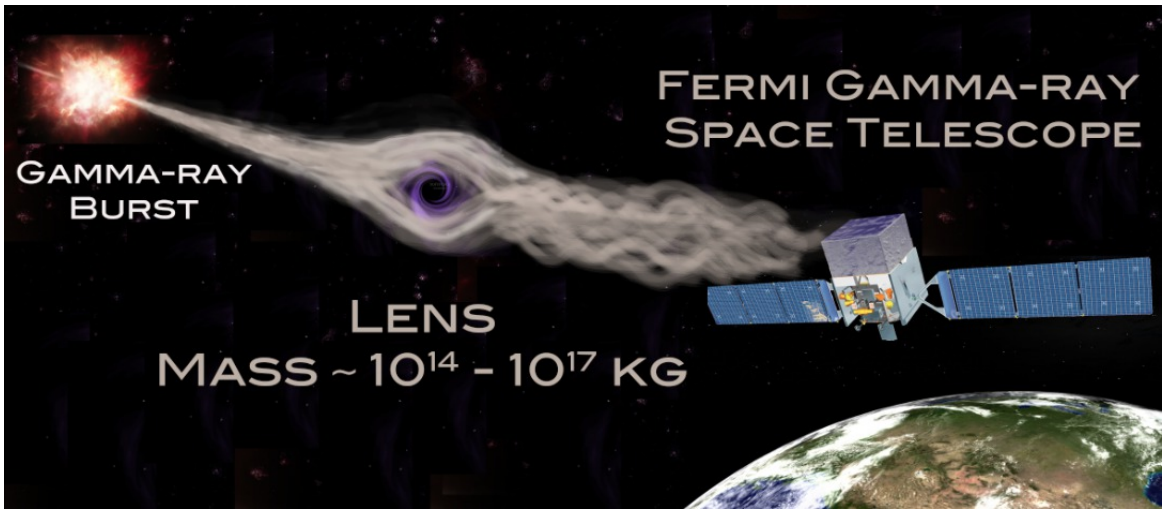

Fig. 1: Schematic picture of a femtolensing phenomena.

2.2 Lensing probability

The optical depth τ for lensing by compact objects is calculated according to the formalism described in Fukugita et al. (1992) [10]. The cosmological parameters used in the calculation are: $\Omega_M = 0.3$ and $\Omega_\Lambda = 0.7$. The calculations are made for both the 111 Friedmann-Lematre-Robertson-Walker (FLRW) and the Dyer-Roeder [11] cosmology. In the sample, the GRB redshift z_s is known. The lens redshift z_L is assumed to be given by the maximum of the $d\tau/dz_L(z_S)$ distribution Fig. 5 of [10]). When $\tau \ll 1$, the lensing probability p is given by $p = \tau\sigma$ where σ is the "lensing cross-section" (see Chap. 11 of [12]).

In this analysis, the cross-section is defined in the following way. Fringes are searched in the spectra of GRBs. These fringes are detectable only for certain positions r_S of the source. The maximum and minimum position of r_S, in units of r_E are noted $r_{S,min}$ and $r_{S,max}$. They are found by simulation and depend on the GRB redshift and luminosity. A minimum value of r_S occurs because the period of the spectral fringes becomes larger than the GBM energy range at small r_S. The femtolensing "cross-section" is then simply

$$\sigma = r_{S,max}^2 - r_{S,min}^2 \,. \tag{4}$$

The lensing probability does not depend on the individual masses of lenses, but only on the density of compact objects Ω_{CO}. In the optical depth calculation, an increase in the mass of the lenses is compensated by a decrease in the number of scatterers. Therefore, the constraints for a given mass depend only on the cross section σ.

3 Data analysis

In our analysis, we use a sample of GRBs detected by GBM with known redshifts. The initial sample consisted of 32 bursts taken from Gruber et al. (2011) [13]. Data were analyzed with the `RMfit` version 33pr7 program. The observed data is a convolution of the GRB photon spectrum with an instrument response function. For each detector with sufficient data, the background was subtracted and the counts spectrum of the first ten seconds of the burst (or less if the burst was shorter) was extracted. The energy spectrum was obtained with a standard forward-folding algorithm. Each burst is then fitted to a standard spectral model.

3.1 Simulations

The detectability of spectral fringes has been studied with simulated signals. The detectability first depends on the luminosity and redshift of the bursts, and second on the detector's energy resolution and data quality. The sensitivity of the GBM to the lens mass M depends strongly also on the energy range and resolution of the GBM detectors. When small masses are considered, the pattern of spectral fringes appears outside of the energy range. The large masses produce fringes with hardly detectable amplitudes and periods smaller than the energy bin size.

Because the data quality and the background are not easily simulated, the detectability estimation is performed on real data. For a given observed GRB, the femtolensing signal depends thus only on 2 parameters: the lens mass M and the source position in the lens plane r_S. The data are then processed as follows:

1. The magnification (equation 2) as a function of the energy is calculated for the given lens mass M and position of the source r_S.
2. This magnification is then convolved with the instrumental resolution matrix to obtain magnification factors for each channel of the detector.
3. The spectral signal is extracted from the data by subtracting the background. It is then multiplied by the corrected magnification.
4. The background is added back.

The detectability calculation can be illustrated with the luminous burst GRB090424592. The spectral data of this burst were first fitted with standard spectral models: BKN, SBKN and BAND. The GRB090424952 burst is best fitted with the BAND model. The fit has $\chi^2 = 78$ for 67 degrees of freedom (d.o.f). The BAND model has 4 free parameters: the amplitude A, the low energy spectral index α, the high energy spectral index β and the peak energy E_{peak}.

The data are then modified by incorporating the spectral fringe patterns for a range of lens masses M and source positions r_S. The simulated data and the corresponding femtolensing fit are presented in figure. 2. Neither BKN nor BAND models are able to fit the simulated data (see

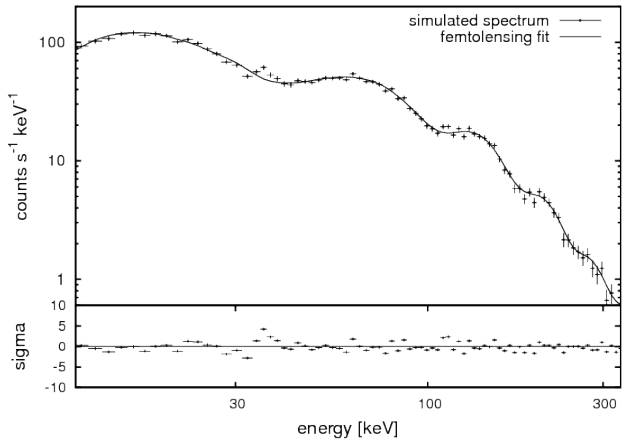

Fig. 2: Simulated spectrum obtained with GRB 090424592. The spectrum was fitted with femtolensing+BAND model. The fit has χ^2 = 79 for 73 d.o.f. The fit parameters are: $A = 0.32 \pm 0.01\,\mathrm{ph\,s^{-1}\,cm^{-2}\,keV^{-1}}$, $E_{peak} = 179 \pm 3\,\mathrm{keV}$, $\alpha = -0.87 \pm 0.02$ and $\beta = -3.9 \pm 7.5$. The simulated femtolensing effect is caused by a lens at redshifts $z_L = 0.256$ and a source at $z_S = 0.544$. The simulated mass is $M = 1 \times 10^{18}$ g and the mass reconstructed from the fit is 1.01×10^{18} g. The source is simulated at position $r_S = 2$. The position reconstructed from the fit is $r_S = 1.9$.

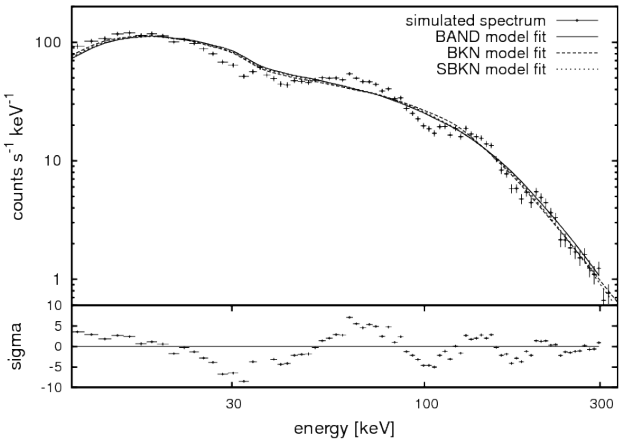

Fig. 3: Simulated femtolensed spectrum fitted with the BAND model. The fit has $\chi^2 = 752$ for 75 d.o.f. The fit parameters are: $A = 0.36 \pm 0.01\,\mathrm{ph\,s^{-1}\,cm^{-2}\,keV^{-1}}$, $E_{peak} = 174 \pm 5\,\mathrm{keV}$, $\alpha = -0.8 \pm 0.02$ and $\beta = -2.4 \pm 0.1$. The S-BKN model fit is almost indistinguishable from the BKN model fit.

figure 3). The values of r_S are then changed until the χ^2 of the fit obtained is not significantly different from the χ^2 of the unmodified data. More precisely, the χ^2 difference $\Delta\chi^2$ should be distributed in the large sample limit as a χ^2 distribution with 2 degrees of freedom according to Wilk's theorem [**?**]. The value $\Delta\chi^2 = 5.99$, which corresponds to a χ^2 probability of 5% for 2 d.o.f, was taken as the cut value.

The pattern in energy is visible when the phase shift between the two images $\Delta\phi \sim (E/1MeV)\left(M/1.5 \times 10^{17}\,g\right)$ is close to 1.

The GBM detector can detect photons with energy from few keV to $\sim$ MeV. Lens masses from 10^{17} g to 10^{20} g are thus detectable with GBM. The femtolensing pattern can be detected when the period of the fringes is larger than the detector energy resolution and smaller than the detector energy range. The value of $r_{S,max}$ comes from the comparison of the period of the oscillating pattern to the detector energy resolution. The value of $r_{S,min}$ arises from the comparison of the period of the fringes to the detector energy range. Because of these constraints, the most sensitive mass range is $10^{18}\,g$ to 10^{19} g.

Figure 4 shows the maximum and minimum detectable r_S for different lens masses. The maximum difference between $r_{S,max}$ and $r_{S,min}$ is at $M = 1 \times 10^{18}$ g. The largest femtolensing cross-section occurs for this mass.

4 Results

The sample of 20 selected bursts have been fitted with the standard BKN, BAND and SBKN models. The models with the best χ^2 probability were selected. The bursts are well fitted by these standard models, so there is no evidence for femtolensing in the data.

As explained in section 2.2, the lensing probability for each burst depends on the lens mass and on the $r_{S,min}$ and $r_{S,max}$ values. Since the sensitivity of GBM to femtolensing is maximal for lens masses of $\sim 1 \times 10^{18}$ g (see figure 4), the values of $r_{S,min}$ and $r_{S,max}$ for each event were first determined at a mass $M = 1 \times 10^{18}$ g by simulation. As explained in section 2.2, the value of $r_{S,min}$ is set by the period of the spectral fringes so that it is independent of the burst luminosity. The lensing probability is then calculated for both the FRLW and Dyer & Roeder cosmological models using the redshift of each burst, the most probable lens position and the values of $r_{S,min}$ and $r_{S,max}$ for the mass $M = 1 \times 10^{18}$ g. The number of expected lensed bursts in the sample is the sum of the lensing probabilities. It depends linearly on Ω_{CO}.

Since no femtolensing is observed, the number of expected events should be less than 3 at 95% confidence level (C.L.). The constraints on the density of compact objects Ω_{CO} is derived to be less than 4% at 95% C.L for both cosmological models. The limits at other lens masses are obtained by normalizing the Ω_{CO} at $M = 1 \times 10^{18}$ g by the cross section σ. The cross section is calculated using equation. (4) and the values of $r_{S,min}$ and $r_{S,max}$ from figure 4. The limits on Ω_{CO} at 95% C.L. are plotted in figure 5.

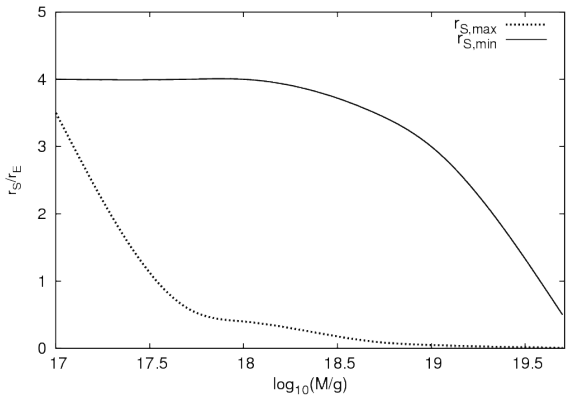

Fig. 4: Minimum and maximum detectable r_S/r_E as a function of the lens mass for GRB 090424592.

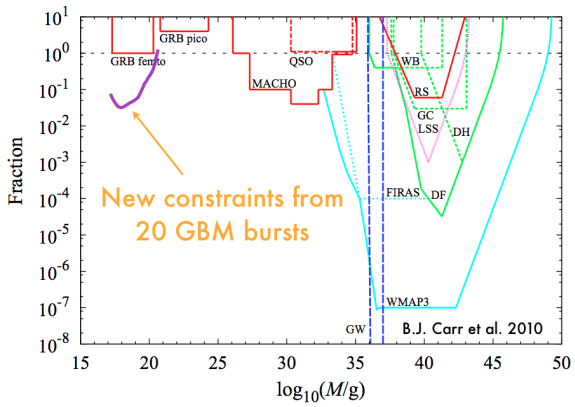

Fig. 5: Constraints on the fraction of compact objects of different masses. Figure credited from [4]

5 Discussion and conclusions

Cosmological constraints on the PBH abundance are reviewed by [4]. One way to obtain the abundance of PBH is to constrain the density of compact objects Ω_{CO}. Note that the limits on the compact object abundance in the $10^{26} - 10^{34}$ g range obtained with microlensing are at the 1% level (MACHO in figure 5). In the mass range below 5×10^{14} g, Ω_{CO} is constrained by PBH evaporation. Above the femtolensing range, the constraints come from microlensing.

It is stated in [14] that the compact objects abundance in the mass range $10^{16}\,\mathrm{g} < M_{BH} < 10^{26}\,\mathrm{g}$ was virtually unconstrained.

Indeed, the only published limits were given by just one group ([15]). The limits are shown on figure 5 as GRB femto and pico. Their limits were based on a sample of 117 bright bursts detected by the BATSE satellite. The bursts were searched for spectral features by Briggs et al. (1998) [16]. The constraints reported by Marani et al. (1999) [15] are $\Omega_{CO} < 0.2$ if the average distance to the GRBs is $z_{GRB} \sim 1$ or $\Omega_{CO} < 0.1$ if $z_{GRB} \sim 2$.

The new idea by Griest et al.[17] shows that the microlensing limit could be improved and get constraints down to 10^{20} g with the Kepler satellite observations. The FERMI satellite was launched three and a half years ago. Since then, almost 1000 of GRB were observed with the GBM detector. In many cases data quality is good enough to reconstruct time-resolved spectra. This unique feature is exploited in our femtolensing search by selecting the first few seconds of a burst in data analysis.

Limits from the present analysis were obtained by selecting only those bursts with known redshifts in the GBM data. This reduces the data sample to only 20 bursts. The constraints on Ω_{CO} obtained at the 95% C.L. are shown on figure. 5. These constraints improve the existing constraints by a factor of 4 in the mass range 10^{17} – 10^{20} g.

After ten years of operation, the GBM detector should collect over 2500 bursts. Only a few of the bursts, say 100, will have a measured redshift and sufficient spectral coverage. By applying the methods described in this thesis, the limits will improve by a factor of 5 reaching a sensitivity to density of compact objects down to the 1% level.

Acknowledgments

Part of this research was supported by the Polish Ministry of Science and Higher Education under grant no. DEC-2011/01/N/ST9/06007 and grant no. PMN CTA 1891.

References

[1] S. W. Hawking, Nature **248**, 30 (1974).

[2] B. J. Carr, ArXiv Astrophysics e-prints (2005) **392** , - (2005).

[3] E. Bugaev and P. Klimai, *Phys. Rev.* D **83**, 083521 (2011).

[4] B. J. Carr *et al*, *Phys. Rev.* D **81**, 4019C (2010).

[5] A. Barnacka *et al*, *Phys. Rev.* D **86**, 3001B (2012).

[6] A. V. Mandzhos, Sov. Astron. Lett. **7**, 213 (1981).

[7] A. Gould, ApJ **386**, 5 (1992).

[8] A. Gould, Astronomical Society of the Pacific Conference Series **239**, 3 (2001).

[9] E. W. Kolb and I. I. Tkachev, ApJ **460**, 25 (1996).

[10] M. Fukugita *et al*, ApJ **393**, 3 (1992).

[11] C. C. Dyer and R. C. Roeder, ApJ **180**, 31 (1973).

[12] P. Schneider *et al*, Springer **-**, - (1992).

[13] D. Gruber *et al*, A&A **531**, 20 (2011).

[14] M. A. Abramowicz *et al*, ApJ **705**, 659 (2009).

[15] G. F. Marani *et al*, ApJ **512**, 13 (1999).

[16] M. S. Briggs *et al*, AIPC **428**, 299 (1998).

[17] K. Griest, M. J. Lehner, A. M. Cieplak, and B. Jain, PRL **107**, 1101 (2011).